PCCP

Intercalation-exfoliation processes during ionic exchange reaction from the sodium lepidocrocite-type titanate toward the proton-based trititanate structure

Journal:	*Physical Chemistry Chemical Physics*
Manuscript ID	CP-ART-01-2021-000352.R1
Article Type:	Paper
Date Submitted by the Author:	31-Mar-2021
Complete List of Authors:	Kang , Seongkoo ; Sorbonne Université, PHENIX Durand-Vidal, Serge; Sorbonne Université, PHENIX Badot, Jean-Claude; Chimie ParisTech, Laboratoire de Chimie de la Matière Condensée de Paris Legein, Christophe; Université du Maine, Institut des Molécules et des Matériaux du Mans (IMMM), UMR CNRS 6283 Body, Monique; Le Mans Université, Institut des Molécules et Matériaux du Mans (IMMM), UMR 6283 CNRS Borkiewicz, Olaf; Argonne National Laboratory, X-ray Science Division Dubrunfaut, Olivier; CentraleSupelec, GeePs Dambournet, Damien; Sorbonne Université, PHENIX

ARTICLE

Intercalation-exfoliation processes during ionic exchange reaction from the sodium lepidocrocite-type titanate toward the proton-based trititanate structure

Received 00th January 20xx,
Accepted 00th January 20xx

DOI: 10.1039/x0xx00000x

Seongkoo Kang,[a,b] Serge Durand-Vidal,[a,b]* Jean-Claude Badot,[b,c] Christophe Legein,[d] Monique Body,[d] Olaf J. Borkiewicz,[e] Olivier Dubrunfaut,[f] and Damien Dambournet [a,b]*

Topochemical reaction involving ionic exchange has been used to assess a large number of metastable compositions, particularly in layered metal oxides. This method encompasses complex reactions that are poorly explored, yet of prime importance to understand and control the materials' properties. In this work, we embark on investigating the reactions involved during the ionic exchange between a layered Na-titanate (lepidocrocite-type structure) and an acidic solution (HCl), leading to a protonic (H_3O^+) titanate (trititanate structure). The reactions involve an ionic exchange provoking a structural change from the lepidocrocite-type to the trititanate structure as shown by real-space refinements of *ex situ* pair distribution function data. Mobile Na^+ ions are exchanged by hydronium ions inducing high proton mobility in the final structure. Moreover, the reaction was followed by *ex situ* ^{23}Na and ^{1}H solid-state MAS NMR which allowed, among other things, to confirm that the Na^+ ions are in the interlayer space and to specify their local environment. Strikingly, the ionic exchange reaction induces a progressive exfoliation of the Na-titanate particles leading to 2-5 nm thin elongated crystallites. To further understand the different steps associated with the ionic exchange, the evolution of the electrolytic conductivity, using conductimetric titration, has been monitored upon HCl addition, enabling to characterize the intercalation(H^+)/de-intercalation(Na^+) reactions and assessing kinetic parameters. Accordingly, it is hypothesized that the exfoliation of the particles is due to an accumulation of charges at the particle level in relation to the rapid intercalation of protons. This work provides novel insights into ionic exchange reactions involved in layered oxide compounds.

Introduction

Layered metal oxides have been studied for numerous applications spanning energy storage[1] or solid-state ionic conductors.[2] Within this class of compounds, layered titanium oxide has been widely investigated, particularly those adopting the lepidocrocite-type structure derived from γ-FeOOH, due to its broad compositional versatility.[3] These layered titanates are classically prepared by solid-state reaction between a titanium oxide precursor and an alkali metal salts leading to a structure built from the stacking of layers of edge/corner-sharing TiO_6 octahedra and by an interlayer space accommodating alkali ions balancing charges.[4–7] They can also be synthesized by low-temperature soft chemistry,[8] to form hydrated interlayer space.[9–11]

Layered titanates have been broadly investigated as precursors for the preparation of titanium oxide nanosheets featuring unique properties.[3,12] The synthesis encompasses an ionic-exchange reaction between the alkali ion located within the interlayer space of the layered titanate and hydronium ions (simplified thereafter as protons) from an acidic solution to produce protonic titanate. The latter is then exfoliated by reacting with organic amines to produce nanosheets.[13]

During the ionic exchange reaction, the topochemical reaction can induce the exfoliation of layers[6,14] and the scrolling of the exfoliated sheets into fibrous or tubular morphology.[15] The driving forces of the topochemical ionic exchange involve the difference of the charge density, osmotic pressure, or acid-base reaction.[8,13,14] Yet of prime importance, the detailed reaction mechanism has been less explored than the material's properties. This study aims to fill this gap by providing a detailed understanding of the reactions involved between a sodium titanate and an acidic solution leading to a protonic titanate. In previous work,[16] we investigated the structure of such protonated layered titanate, which consists of a trititanate arrangement with hydronium ions and water molecules stabilized in the interlayer space. This compound displays a high proton conductivity of 4.10^{-2} S/m and interesting intercalation properties with respect to protons in an aqueous battery. Moreover, its morphology is built from the stacking of layers

[a] Sorbonne Université, CNRS, Physico-chimie des Electrolytes et Nanosystèmes Interfaciaux, PHENIX, F-75005, Paris, France.
E-mails : serge.durand-vidal@sorbonne-universite.fr, damien.dambournet@sorbonne-universite.fr
[b] Réseau sur le Stockage Electrochimique de l'Energie (RS2E), FR CNRS 3459, 80039 Amiens, France
[c] Chimie ParisTech, PSL Research University, CNRS, Institut de Recherche de Chimie Paris, 11 rue Pierre et Marie Curie, 75005 Paris, France
[d] Institut des Molécules et Matériaux du Mans (IMMM)- UMR 6283 CNRS, Le Mans Université, Avenue Olivier Messiaen, 72805 Le Mans Cedex 9, France
[e] X-ray Science Division, Advanced Photon Source, Argonne National Laboratory, Argonne, Illinois 60439, United States
[f] GeePs Group of Electrical Engineering – Paris, UMR CNRS 8507, CentraleSupélec, Sorbonne Université, Univ Paris-Sud, Université Paris-Saclay, 11 rue Joliot-Curie, 91192 Gif-sur-Yvette, France

† Footnotes relating to the title and/or authors should appear here.
Electronic Supplementary Information (ESI) available: additional characterizations including FT-IR, TGA, PDF analysis, BDS, TEM, SEM, AFM, solid-state NMR. See DOI: 10.1039/x0xx00000x

with a thickness of 3-5 nm, an interesting feature for the synthesis of titanium oxide nanosheets. In this work, the mechanisms driven by the ionic-exchange reaction are investigated with focusses on the structural/compositional/morphological changes. We provide new insights on these changes highlighting a concomitant intercalation(H^+)/de-intercalation(Na^+) reaction and exfoliation mechanism as evidenced by *ex situ* and *in situ* measurements enabling us to gain new knowledge on this class of materials.

Experimental

Synthesis

In a Teflon-lined container, we mixed 4 mL of Ti (IV) isopropoxide (> 97 %, Sigma-Aldrich) and 26 mL of 10 M NaOH under stirring. The mixture was then sealed in a stainless-steel autoclave and a thermally activated precipitation was performed at 90 °C for 12 h.[16] The obtained white precipitate was washed two times with 30 mL of demineralized water to remove residual species such as NaOH. Na-titanate was then dried at 80 °C overnight under vacuum.

To better understand the ion-exchange reaction of Na-titanate with HCl, we collected the samples at different pH values (9, 7, 4, and 2) by using different HCl concentrations. Typically, the dispersion was left under stirring for 20 min until the pH was stabilized. The precipitate was then washed with demineralized water and dried at 80 °C overnight.

X-ray diffraction and Synchrotron X-ray Scattering

The powder X-ray diffraction data were collected using a Rigaku diffractometer equipped with Cu Kα radiation.

High-energy X-ray (λ = 0.2128 Å) synchrotron scattering was performed at the 11-ID-B beamline of the Advanced Photon Source at Argonne National Laboratory. 1D diffraction data were obtained using Fit2D to integrate 2D total scattering data.[17] Extractions and refinements of pair distribution functions (PDFs) were performed using respectively PDFgetX3,[18] and PDFgui.[19]

Conductometric and pH titration

Dried Na-titanate powder (0.1 g) was dispersed in demineralized water (16 mL) and the mixture was stirred to homogenize the solution. We performed subsequent additions of 0.1 mL of 1 M of HCl and then measured *in situ* the conductivity at room temperature. The pH was measured *ex situ* due to the interference between the probe of the conductivity meter and the pH electrode. We used KEYSIGHT E4990A Impedance Analyser (20Hz-50MHz) and a Ficher Bioblock Scientific four-points conductivity probe (cell constant close to 10 cm^{-1}). Preliminary frequency scans were performed between 100 Hz and 10 MHz in the mixtures under stirring. The imaginary part of the impedance being close to zero at 5 kHz, the titrations were performed at this frequency.

Broadband dielectric spectroscopy

The complex conductivity and dielectric permittivity measurements were performed between 50 and 10^{10} Hz by coupling Agilent E4990A Impedance Analyzer (50 to 10^8 Hz) and Agilent E8364B PNA Network Analyzer (10^7 to 10^{10} Hz). The sample pellets (diameter = 3 mm, thickness = 1 mm) were prepared by pressing at 0.7 GPa and metallized with silver paint. The pellet was placed between a short-circuit and an inner conductor of a coaxial APC7 cell.[20]

FT-IR

Infrared spectra of the samples were measured using a Bruker Equinox 55 spectrometer equipped with ATR diamond crystal accessory, a Ge/KBR beamsplitter, and a liquid nitrogen-cooled MCR detector under ambient conditions and with a spectral resolution of 4 cm^{-1}.

Microscopy and Energy Dispersive X-ray Spectroscopy

The transmission electron microscopy experiments were performed using a JEOL 2100 Plus UHR microscope at 200 kV equipped with a TCD camera. The scanning electron microscopy and the energy dispersive X-ray spectroscopy (EDX) analysis were performed with Hitachi Su-70 at 5 kV and Oxford X-Max 50 mm^2.

Thermogravimetric Analysis

The Thermogravimetric experiments analysis was performed using a TA instrument TGA550 analyzer from 25 °C to 600 °C (heating rate of 1 °C/min) under N_2 atmosphere.

^{1}H and ^{23}Na solid-state MAS NMR

^{1}H (I = 1/2) and ^{23}Na (I = 3/2) solid-state magic angle spinning (MAS) NMR experiments were performed using a Bruker Avance 300 spectrometer operating at 7.0 T (^{1}H and ^{23}Na Larmor frequencies of 300.2 MHz and 79.4 MHz, respectively), with a 1.3 mm CP-MAS probe head. The room temperature ^{1}H and ^{23}Na MAS spectra were recorded using a Hahn echo sequence with an interpulse delay equal to one rotor period.[21] The 90° pulse length were set to 2.4 µs and 2.375 µs, respectively. 160 and 8 k or 48 k transients were accumulated with recycle delays of 20 s and 1 s, respectively. ^{1}H and ^{23}Na spectra are referenced to TMS and 1 M NaCl solution, respectively and were fitted using the DMFit software.[22]

Atomic force microscopy (AFM)

Drops of H-titanate suspension were let dry on a freshly cleaved green mica (1 cm^2) at ambient temperature. The images of the surfaces were obtained using TM AFM on a Nanoscope III from Digital Instruments. A Si – n tip whose curvature radius is in the range of 5 – 30 nm was used. The spring constant of the tip is in the range 30– 100 N/m, and the resonance frequency in the range 200 – 400 kHz.

Results & Discussions

Pristine Na-titanate

Na-titanate was prepared by reacting $Ti(OiPr)_4$ with concentrated NaOH (10 mol.L^{-1}) under hydrothermal conditions (see experimental section). The obtained precipitate is particularly moisture sensitive and was isolated by washing the powder with a defined amount of demineralized water (see experimental section). We note that increasing the amount of water initiates the extraction of Na^+ ions.

The structure of the pristine Na-titanate was characterized after a mild drying. The XRD pattern of Na-titanate shown in **Fig. 1**, features broad Bragg peaks characteristic of nanosized particles and/or disordered structure.

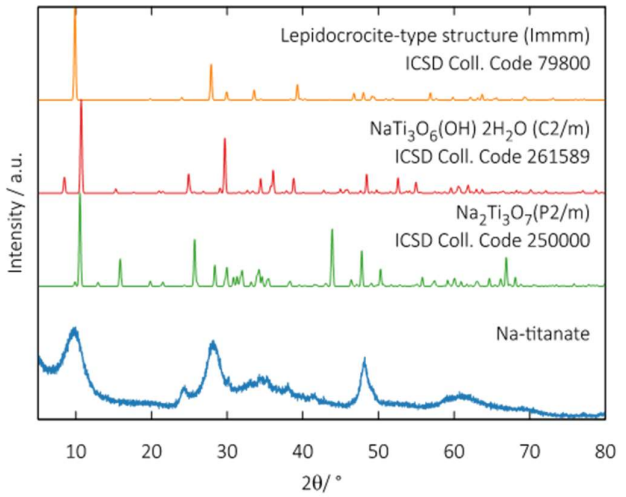

Fig. 1 XRD patterns of as-prepared Na-titanate and reference compounds.

The Bragg peak located at ~10° (2θ) is primary indicative of a layered-type structure as found in the lepidocrocite[13], or in the layered sodium titanate.[23,24] The layers of the lepidocrocite are composed of edge-sharing TiO_6 octahedra (Fig. S1a). The layered sodium titanate, denoted sodium trititanate, is composed of corrugated ribbons of edge-sharing TiO_6 octahedra. The ribbons built from three octahedra, are connected by corner-sharing (Fig. S1b). Small peaks were observed between 30 and 50° (2θ) and were assigned to Na_2CO_3 as further evidenced by FT-IR spectroscopy (**Fig. S2**). The presence of sodium carbonate might be due to a carbonation reaction during the drying process. According to thermal analysis and FT-IR spectroscopy, the phase is hydrated. A significant contribution of interlayer water is demonstrated by the bands around 3400 cm^{-1} and 1653 cm^{-1} corresponding to the stretching and the bending modes of O–H bonds of water molecules, respectively (**Fig. S2**). Moreover, the thermal behavior assessed by TGA analysis (**Fig. S3**) is similar to that observed for the protonated lepidocrocite $H_xTi_{2-x/4}\square_{x/4}O_4.nH_2O$.[13]

To identify the structure of Na-titanate, high-energy X-ray synchrotron total scattering data were collected and Fourier-transformed to pair distribution function (PDF), which represents a histogram of all atomic pair distances.[25] The experimental PDF was refined using different structural models (**Fig. S4**). The lepidocrocite structure (*Immm*, a = 3.803 Å, b = 18.692 Å , c = 3.067 Å, $\alpha = \beta = \gamma = 90°$)[13] provided the most suited model (**Fig. 2**). The difference curve, however, displays residual features assigned to inter-atomic distances that cannot be captured by the structural model (see for instance, the peak at 2.29 Å). The reason for it is that the model includes only Na^+ and O^{2-} ions located within the interlayer space (**Inset of Fig 2**) but includes neither Na-O distances arising from Na^+ ions solvated by water molecules nor Na^+ ions possibly located within the titanate layer. From a thermodynamic perspective, the occupation of Na^+ ions within the interlayer is only 20 meV more stable than in the titanium layer.[26] The general chemical formula of the Na-titanate is $Na_xTi_{2-x/4}\square_{x/4}O_4.nH_2O$, where Na^+ ions most likely occupy the interlayer space, *i.e.*, solvated by water molecules, and within the titanate layer.

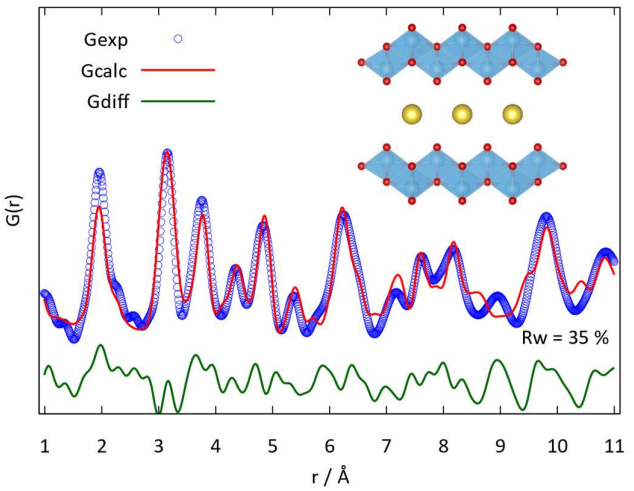

Fig. 2 Real-space refinement of the PDF data of Na-titanate using the lepidocrocite (S.G: *Immm*) as a structural model. Blue dots, red and green curves represent experimental, calculated and difference curves. Inset: structural representation of the Na-titanate, the structural water molecules are not included.

To assess the chemical composition of the Na-titanate, we combined conductimetric titration (see experimental section and below), thermal analysis, and EDX analysis (Na/Ti = 0.89), leading to $(NaOH)_{1.1}Na_{0.56}Ti_{1.86}\square_{0.14}O_4{\cdot}1.38H_2O$. The results point to the presence of residual NaOH probably trapped within the aggregates of particles, which can further react with CO_2 to produce Na_2CO_3 as revealed by XRD.

To understand the ionic exchange reaction from Na-titanate to H-titanate, we used dielectric spectroscopy to assess ionic mobility and water dynamic within the Na-titanate. At first, we determined the bulk ionic conductivity of the Na-titanate (**Fig. S5**) with a value of $1.5{\cdot}10^{-3}$ S/m. While this value is about 30 times lower than that of H-titanate, it reveals that Na-titanate displays ionic mobility.

The complex permittivity was then used to identify the relaxations of local charge motions, which encompass the rotation of water, the charge hopping at high frequency, and the grain polarizations at low frequency.[27] The Nyquist plots of the imaginary part of the complex permittivity $\varepsilon''(\omega)$ *vs*. the real

part *ε'(ω)* recorded at room temperature between 50 and 10^{10} Hz are represented in **Fig. 3a**. In the whole diagram, only the low-frequency contribution P1 (P stands for part) was observed by fitting the experimental data with an inclined straight line. P1 can be attributed to the sample conductivity and the double-layer capacitance. Due to the much larger amplitude of low-frequency contribution P1, high-frequency relaxations are obtained by decomposing the experimental data. We identified three high-frequency relaxations, P2 (**Fig. 3b**), P3 (**Fig. 3c**), and P4 (**Fig. 3d**), which are all fitted with the Cole-Cole function.[28] P2, P3, and P4 are respectively attributed to grain polarization, ionic motion, and interlayer water rotation.

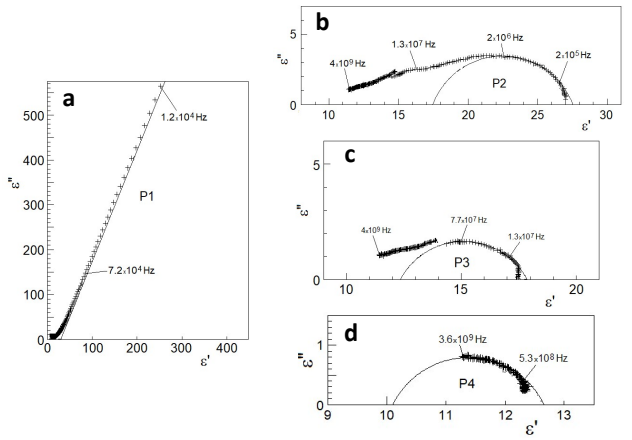

Fig. 3 Nyquist plots of permittivity at RT: a) Entire plot with the low-frequency contribution P1 (straight line); b) plot obtained upon subtracting the contribution P1 and evidence of the relaxation domain P2; c) plot obtained upon subtracting the domain P2 and evidence of the relaxation domain P3; d) plot obtained upon subtracting the domain P3 and evidence of the relaxation domain P4.

The relaxation frequencies of each contribution were gathered in **Table 1** and compared with the data of H-titanate[16]. The activation energies E_A of Na-titanate were not given because the measurements at different temperatures were not performed on this sample. The grain polarization of Na-titanate was observed at $2.0 \cdot 10^6$ Hz, which is in the same order of magnitude as H-titanate. The relaxation frequency attributed to the charge hopping was found at $7.7 \cdot 10^7$ Hz for Na-titanate, about two times lower than the charge hopping in the H-titanate. We can reasonably attribute the charge to the interlayer Na^+. Na^+ ion hopping in V_2O_5 gels was detected at a similar frequency, around 10^8 Hz at 300 K.[29] We note that for a confident attribution of the origin of the charge, the activation energy of this relaxation should have been defined. The last relaxation evidenced at $3.6 \cdot 10^9$ Hz is related to the rotation of the interlayer water. Considering the relaxation frequency of the bulk water[30] ($18 \cdot 10^9$ Hz), P4 of Na-titanate can be attributed to confined water whose rotation is slowed down by the presence of Na^+ ions.[29] Hence, BDS measurements suggested that Na^+ ions and water molecules are mobile within the Na-titanate, further promoting ionic exchange reaction.

Characterization of ionic exchange by *ex-situ* analysis

To better understand the structural and morphological changes occurring during the ionic exchange, we prepared different samples featuring a tunable content of Na^+-H^+. Samples of Na-titanate were treated with solutions having different concentrations of HCl. The dispersion was left under stirring for 20 min until the pH was stabilized. The corresponding pH was 9, 7, 4, and 2. The samples obtained were analyzed by XRD and TEM (**Fig. 4**).

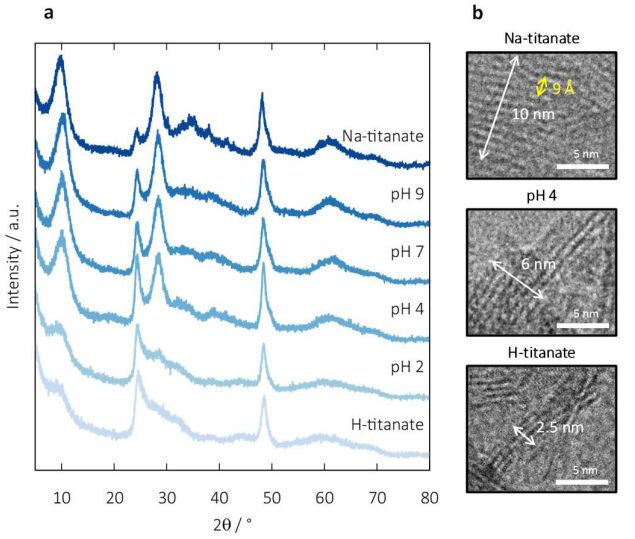

Fig. 4 a) The XRD patterns and b) TEM images of the samples collected at different pH during acid treatment of Na-titanate.

Table 1. Frequency and attribution of dielectric relaxations observed at the high-frequency region to grain polarization (P2), ionic motion (P3) and interlayer water rotation (P4) and grain conductivity for Na-titanate and H-titanate.

	Contribution	P2	P3	P4
Na-titanate	Frequency / Hz	$2.0 \cdot 10^6$	$7.7 \cdot 10^7$	$3.6 \cdot 10^9$
	Conductivity/S.m^{-1}	$1.5 \cdot 10^{-3}$		
H-titanate	Frequency/Hz	$1.1 \cdot 10^6$	$1.6 \cdot 10^8$	$2.2 \cdot 10^9$
	Conductivity/S.m^{-1}	$4.0 \cdot 10^{-2}$		

Upon Na^+-H^+ exchange, the evolution of the XRD patterns (**Fig. 4a**) shows a progressive structural transformation from the Na-lepidocrocite to the proton trititanate structure. The phase transition is accompanied by a progressive broadening of X-ray peaks, particularly for the first peak located at 2θ~10°. The peak broadening can be due to either or both the effect of morphology or/and the structural disorder. Transmission and scanning electron microscopy (**Fig. 4b, S6, S7**) revealed that the ionic Na^+-H^+ exchange is accompanied by an exfoliation of the particles. For the Na-titanate, we observed aggregates of nanoparticles (**Fig. S6a, S7a**) composed of stack of layers with a thickness of 10 nm (**Fig. 4b, S6c**) and a lattice plane separation of 9 Å corresponding to the d_{002} spacing of the lepidocrocite structure. This corresponds to the stacking direction of the layered structure. Upon Na^+-H^+ exchange, we observed a continuous decrease of the particle's thickness. The number of slabs decreases to six at pH 4 up to 2-5 layers for the H-titanate (**Fig. 4b**). Hence, we concluded that the Na-titanate to H-

titanate transformation was accompanied by exfoliation of layers producing 1D morphology (**Fig. S7b, S8**) of around 2-5 nm thickness. The decrease of the thickness of 1D morphology is clearly observed by comparing the TEM images before and after the acid treatment (**Fig. S6c, d**). In addition, the fragments of the exfoliation are found in the TEM images of H-titanate (red circles, **Fig. S7b**). The observed broadening of the first Bragg peak is then attributed to the decrease of the particle dimension along the *c*-axis. We also note a decrease in the particles' agglomeration.

The evolution of the short-range order of the samples prepared at different pH values was analyzed using PDF (**Fig. 5**). The PDFs showed peak intensities starting to decrease above 20 Å, which is primarily related to finite-size effects.[33] Upon ionic exchange, we observed noticeable changes in peak intensity, particularly at low inter-atomic distances $r < 4$ Å. The three first peaks are respectively assigned to Ti–O, edge-sharing Ti···Ti, and corner-sharing Ti···Ti distances. The changes in intensity for the second and third peak are attributed to the phase transformation from the lepidocrocite (Na-titanate) to the trititanate structure (H-titanate) as shown by XRD analysis.[34] Moreover, we observed the disappearance of the shoulder at around 2.26 Å tentatively assigned to Na^+ ions solvated by water molecules and/or located within the titanate slab.[26]

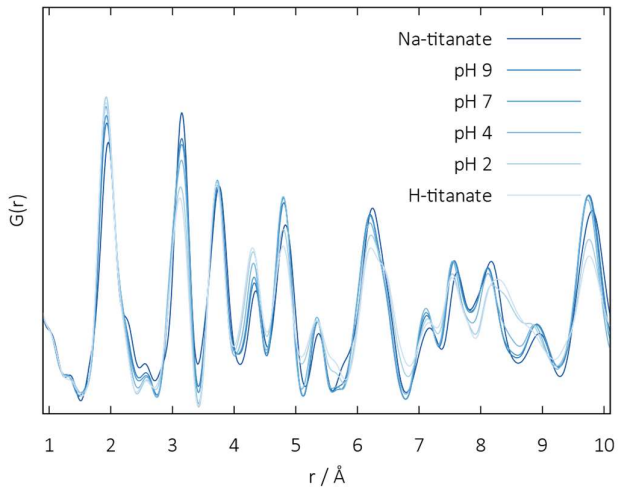

Fig. 5 X-ray PDFs of Na-titanate, H-titanate and the samples collected at different pH values.

To follow the structural transition from Na-titanate (lepidocrocite) to H-titanate (trititanate), we refined the PDF data of the samples prepared at different pH values. We used a two-phase model to quantify the content of each phase upon gradual Na^+-H^+ ionic exchange. The corresponding refinements are gathered in **Fig. S9** and **Fig. S10**. Quantitative phase analysis as a function of the pH was plotted in **Fig. 6**. Upon ionic exchange, the amount of lepidocrocite-type structure gradually decreases while the content of trititanate increases. At pH 4, the two phases coexist in almost the same proportion and a full conversion is complete only at pH 1. Hence, we concluded that the ionic exchange induces a phase transition of the Na-lepidocrocite toward the proton-based trititanate structure. The transition from a flat edge-sharing TiO_6 octahedra lepidocrocite toward the corrugated ribbons of edge-sharing TiO_6 octahedra as found in the trititanate arrangement suggested that upon ionic exchange, the structure undergoes an atomic re-organization. Such a change might be induced by the presence of cationic vacancies in the Na-based titanate ($Na_{0.56}Ti_{1.86}\square_{0.14}O_4$) as these vacancies are absent in the trititanate structure ($(H_3O)_{1.35}Ti_3O_{6.67}\square_{0.33}$. Moreover, it is well known that the nature of the intercalated species drastically affect the structure of layered titanates, which is consistent with the phase transition observed here.[31,32]

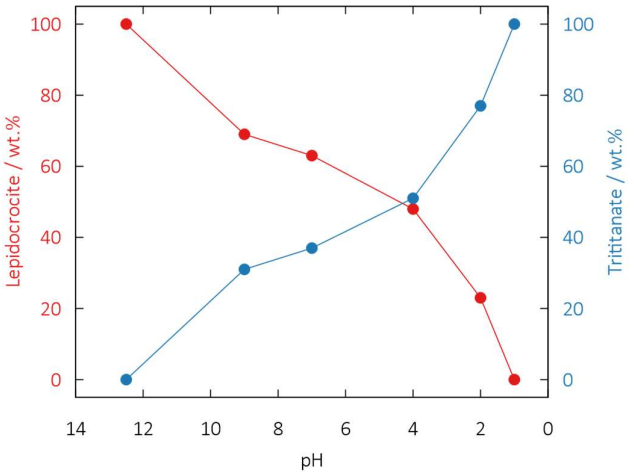

Fig. 6 Quantitative phase analysis obtained by real-space refinements of the samples collected at different pH values.

Owing to its sensitivity to the local atomic-scale structure, solid-state MAS NMR was used to probe the environments of the sodium and hydrogen atoms in the samples prepared at different pH values (**Fig. 7**, fits of the spectra are given as ESI). The ^{23}Na NMR spectra consist of a broad line whose shape is characteristic of disordered sodium sites and their reconstruction was achieved considering the GIM model, *i.e.*, a Gaussian distribution of isotropic chemical shifts and distribution of quadrupolar interactions (**Fig. S11** and **Table S1**). The NMR parameter distributions used to reconstruct the spectra reveal disorder around Na^+ ions. In agreement with PDF refinements and energy-dispersive spectroscopy (**Fig. S12**), a strong decrease of the peak intensity is observed when the pH decreases, especially below pH 7 (**Fig. 7 and S13**).

The average isotropic chemical shift $<\delta_{iso}>$ is around -12 ppm at pH = 9. Similar values were measured/observed in $Na_2Ti_3O_7$ and $Na_2Ti_6O_{13}$ but, in these two compounds, the coordination number (CN) of the Na^+ ions assigned to these $<\delta_{iso}>$ values are 9 and 8, respectively.[35,36] However, the CN of the cationic vacancies is 6 and if the Na^+ ions occupied them, higher δ_{iso} values should be observed since an increase of δ_{iso} is usually noticed for decreasing oxide ion CN and mean Na–O distance.[37] This confirms that Na^+ ions are localized in the interlayer space and coordinated by oxygen atoms of water molecules since ^{23}Na

NMR resonances of hydrated Na^+ ions in layered oxides were observed at similar δ_{iso} values.[38–40] Considering the initial molar H_2O/Na ratio (~2.5) and the corresponding $<\delta_{iso}>$ value, a CN of 2 seems to be a realistic hypothesis. Indeed, for $Na(H_2O)_n^+$ species, δ_{iso} decreases with n[41] and the δ_{iso} value for $Na(H_2O)_6^+$ (shift reference) is 0.0 ppm. Whereas the Na^+-H^+ ionic exchange results in an increase of the molar H_2O/Na ratio, the $<\delta_{iso}>$ values remain constant up to pH = 2 included (**Table S1** for 9 ≤ pH ≤ 4 and $<\delta_{iso}>$ ~ -12.8 ppm for pH = 2). On the other hand, for pH = 1 the fit (not shown) leads to a value of $<\delta_{iso}>$ ~ -3 ppm and this significant increase of $<\delta_{iso}>$ clearly indicates a significant increase in the CN of the Na^+ ions. The disorder around Na^+ ions can be related to variation in the distances with the oxygen atoms of the H_2O molecules.

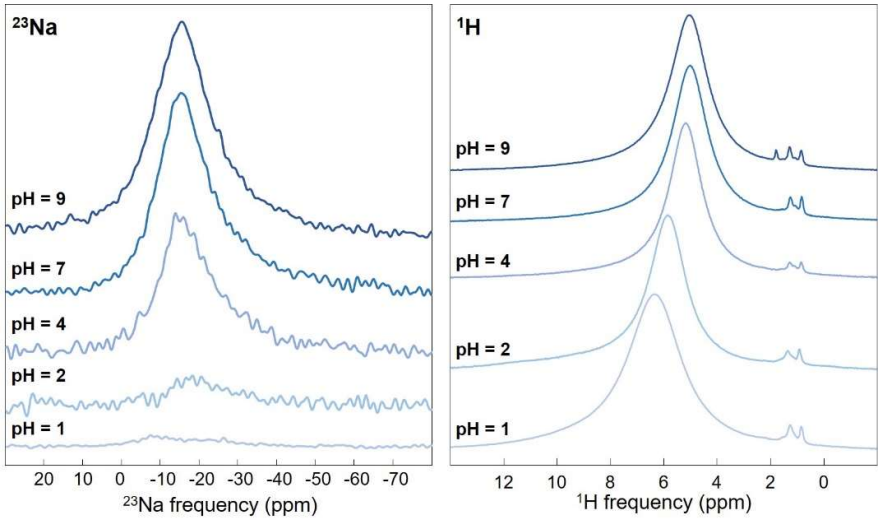

Fig. 7 a) ^{23}Na non-normalized and ^1H (normalized) MAS (44 and 60 kHz, respectively) NMR spectra of the samples collected at different pH values. The ^{23}Na non-normalized spectra correspond, for each sample, to the same number of scans and the same sample mass in the rotor so that the areas under the curves can be directly compared.

The ^1H MAS NMR spectra consist of a broad contribution more or less asymmetric (two or three lines are needed to reconstruct them properly) and some narrow and small resonances in the range 0.8 to 1.4 ppm that can be assigned to a small amount of terminal OH groups, Ti–OH[11,42] (**Fig. 7b**, **S14** and **Table S2**). The Na^+-H^+ ionic exchange results in an increase in the $<\delta_{iso}>$ value (from 5.3 to 6.6 ppm) and to a broadening of the main contribution. These results are consistent with the exchange since it leads to an increase in the quantity of hydronium ions whose δ_{iso} value (9 ppm in zeolites[43]) is higher than that of water. The respective contributions of water and hydronium ions are difficult to distinguish and therefore quantify. As in the case of another layered titanate,[16] it can then be assumed that resonances of H_3O^+ ions and H_2O molecules, broadened by disorder and residual dipole coupling, merge because of the rapid exchange of protons between these species.

Characterization of ionic exchange by *in situ* conductometric and pH metric measurements

Ion exchange process. To better understand the Na^+-H^+ ionic exchange, we used conductometric titration which, allows us to measure the change in electrolytic conductivity.[44,45] The species involved during the Na^+-H^+ ionic exchange that are H^+ (H_3O^+), Na^+, Cl^- and OH^- ions, showed remarkable differences in ionic molar conductivities (**Table 2**). Notably, the molar conductivities of exchanged Na^+-H^+ ions differ by a factor of 7. Moreover, the conductivity measurement is almost instantaneous at a fixed frequency enabling to obtain kinetic information. Finally, reaction mechanisms can be investigated by comparing the experimental and calculated ionic conductivities. The latter can be assessed by the following formula:

$$\sigma = \sum \lambda_n^0 C_n$$

where λ_n^0 and C_n represent the ionic molar conductivity at infinite dilution and the concentration of each ion, respectively. This formula is only valid when the interactions between ions are negligible, *i.e.*, when the ionic solution is very dilute, which was valid during the entire titration until a great excess of HCl was introduced at the end. Powder of Na-titanate was dispersed in demineralized water and the ionic conductivity of the solution was monitored upon addition of aliquots of HCl (see experimental section). The corresponding conductivity and pH curves are shown in **Fig. 8**. After the dispersion of Na-titanate in demineralized water, the pH increases to 12.4, which agrees with the amount of synthetic residual of NaOH. The evolution of the conductivity can be divided into three different regions marked on the top side of **Fig. 8**. Within the first region, the conductivity features a pattern consisting of an immediate decrease followed by a plateau. Such a feature is consistent with an acid-base reaction between added HCl and residual NaOH. To confirm this assumption, we calculated the expected evolution of the conductivity relying on an acid-base reaction as detailed below.

At t = 0 s, the initial conductivity is related to residual NaOH and the conductivity can be calculated with equation 1. The deduced NaOH concentration was 0.033 M. Just after the first addition of HCl, the conductivity of the solution can be expressed by equation 2. Thereafter, the acid-base reaction occurring between OH^- and H^+ ions is represented by equation 3. When all OH ions were neutralized, the conductivity can be calculated with equation 4.

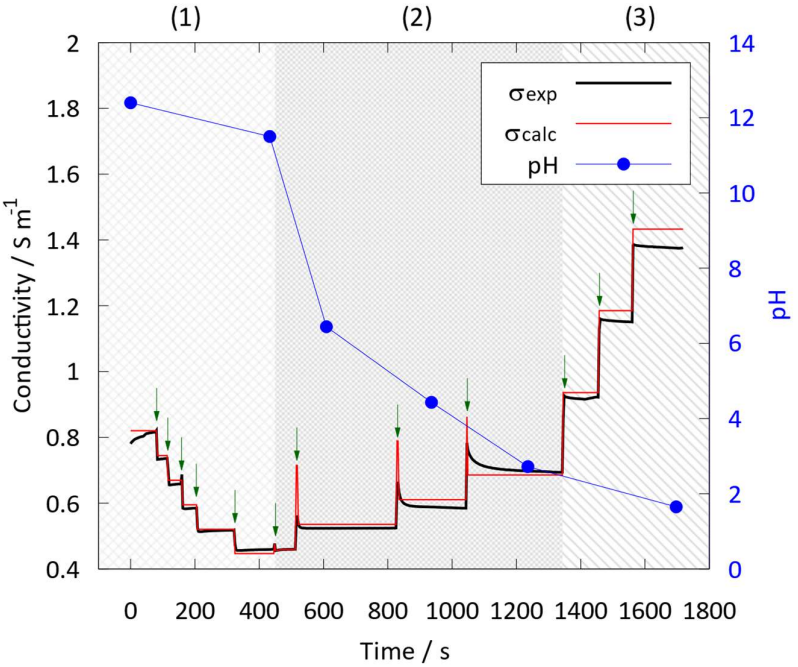

Fig. 8 Evolution of the ionic conductivity (black) and pH (blue curve) upon addition of aliquots of HCl_{aq}. The green arrow refers to the addition of 1 mL of 1 M HCl. The red curve corresponds to the calculated ionic conductivity.

$$\sigma_{(1)} = \lambda^0_{Na+}[Na^+]_i + \lambda^0_{OH-}[OH^-]_i \quad (1)$$

$$\sigma_{(2)} = \sigma_{(1)} + \lambda^0_{H+}[H^+]_{add} + \lambda^0_{Cl-}[Cl^-]_{add} \quad (2)$$

$$\sigma_{(3)} = \lambda^0_{Na+}[Na^+]_i + \lambda^0_{OH-}([OH^-]_i - [H^+]_{add}) + \lambda^0_{Cl-}[Cl^-]_{add} \quad (3)$$

$$\sigma_{(4)} = \lambda^0_{Na+}[Na^+]_i + \lambda^0_{Cl-}[Cl^-]_{add} \quad (4)$$

As the ionic molar conductivity of OH^- is higher than Cl^-, the conductivity is expected to decrease after the acid-base reaction. The calculated conductivity corresponding to the acid-base reaction is in good agreement with the experimental values, confirming our hypothesis. We note, however, that in the experimental curve, the increase of the conductivity related to equation 2 is absent, which is due to the fast kinetics of the acid-base reaction.

In the second region, the ionic exchange is characterized by a strong decrease of the pH from 11.5 to 2.3, which corresponds to the phase transition from Na-titanate to the H-titanate as shown by *ex situ* analysis. At each addition, the conductivity features a rapid increase due to the presence of protons (eq. 5), followed by a decrease up to a plateau region. Such a decrease is associated with the disappearance of H^+ from the solution, *i.e.*, protons are diffusing from the solution to the structure while Na^+ ions are de-inserted and release in the solution (equation 6).

$$\sigma_{(5)} = \sigma_{(4)} + \lambda^0_{H+}[H^+]_{add} + \lambda^0_{Cl-}[Cl^-]_{add} \quad (5)$$

$$\sigma_{(6)} = \sigma_{(4)} + \lambda^0_{Na+}[Na^+]_{rlse} + \lambda^0_{Cl-}[Cl^-]_{add} \quad (6)$$

The evolution of the experimental conductivity during the second region is in good agreement with the calculated values confirming that Na^+–H^+ exchange reactions are the dominant process. We note, however, a discrepancy between the experimental and calculated values upon the stabilization of the conductivity. This is due to kinetic effects as further discussed below.

Table 2. Ionic molar conductivities at infinite dilutions at 25 °C of ions involved in the acid treatment.

Ions	Ionic molar conductivities at infinite dilutions (cm^2 S mol^{-1})
H^+	349.65
Na^+	50.08
Cl^-	76.31
OH^-	198.00

During the third region, the pH decreases only slightly from 2.3 to 1.9 showing that the reaction is completed. Hence, the variation of the conductivity is only due to the addition of HCl (equation 7). Indeed, the conductivity increases and stabilizes after the addition of HCl.

$$\sigma_{(7)} = \sigma_{(6)} + \lambda^0_{H+}[H^+]_{add} + \lambda^0_{Cl}\ [Cl^-]_{add} \quad (7)$$

We note that the difference between the calculated and experimental conductivity increases upon adding HCl. At high concentrations, the ionic conductivity becomes affected by ion-

interactions, *i.e.*, an increase of the ionic strength. Hence, the law used to describe the ionic conductivity is no longer accurate.[46,47]

Kinetic aspect. In the second region assigned to the phase transition from Na-titanate to the H-titanate, we observed a gradual conductivity decrease not captured by the calculated ionic conductivity highlighting kinetic effects (**Fig. 9a**). To better visualize such effects, we normalized the conductivity decays as shown in **Fig. 9b**. During the three addition of HCl aliquots, the decays increase from 47 s to 202 s and 266 s, emphasizing a decrease of the Na^+-H^+ reaction kinetics.

To capture the reaction kinetic effects, we modified the expression of the ionic conductivity as found in equation 5 and added an exponential function $F(t)$ (equation 8).

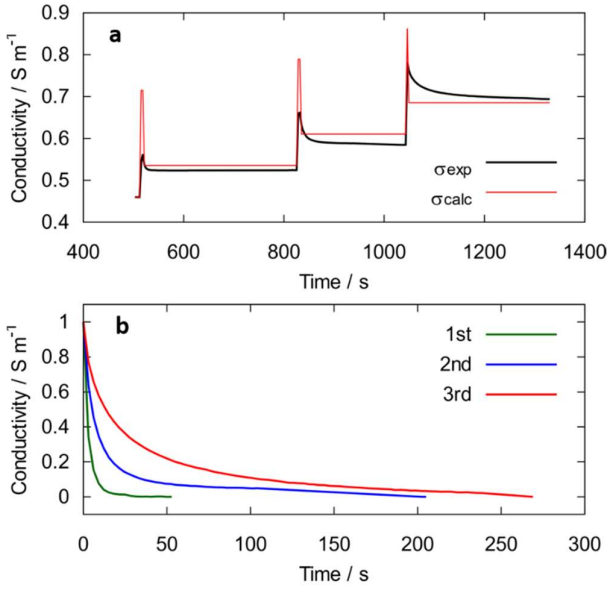

Fig. 9 a) Comparison of the experimental and calculated ionic conductivities during the ionic exchange. b) Normalized conductivity decays upon additions of HCl.

$$\sigma_{(8)}(t) = \sigma_{(5)} - \lambda^0{}_{H+}[H^+]_{ins}(t) + \lambda^0{}_{Na+}[Na^+]_{rlsd}(t) = \sigma_{(5)} - F(t) \quad (8)$$

The function $F(t)$ can be a one or two-exponential function as shown in equation 9.

$$F(t) = Ae^{-t/\tau_A} + Be^{-t/\tau_B} = Ae^{-k_A t} + Be^{-k_B t} \quad (9)$$

where τ_i is the characteristic time of given ion *i*, $k_i = 1/\tau$ is the kinetic constant, and the prefactors *A* and *B* are related to the diffusing ions.

The introduction of the exponential law enabled to fit the decay of the ionic conductivity during the Na^+-H^+ ionic exchange (**Fig. S15**). We note, however, that the first addition was fitted using a mono-exponential law while the second and third additions were fitted using a bi-exponential function. This is indicative of different kinetic regimes. The fitted kinetic constant k_i for each addition are gathered in **Table 3**.

Table 3. Kinetic constants obtained by fitting the decay of the ionic conductivity during the three subsequent additions of HCl.

	k_1 (s^{-1})	k_2 (s^{-1})
1st	0.322	
2nd	0.161	0.015
3rd	0.105	0.013

The model used during the first addition, which is a mono-exponential law, indicates that H^+ diffusion is the dominant process, which can be explained by faster kinetic involving the most accessible sites, *i.e.*, surface sites.

Upon subsequent HCl additions, the decays were fitted with a bi-exponential law leading to distinct kinetic constants.

To account for the two kinetic constants, we followed the work of Bavykin *et al.*[48] (themselves inspired by Dickenson and Fiennes[49]), who considered that the kinetic of ionic exchange reaction involved two main processes that are the diffusion of guest H^+ and host Na^+ ions. Because of the high proton mobility of the final protonic trititanate, we considered that the concentration of the inserted H^+ is different from the concentration of the released Na^+, *i.e.*, $[Na^+]_{released}(t) \neq [H^+]_{inserted}(t)$. We note that for a different hypothesis assuming that $[Na^+]_{released}(t) = [H^+]_{inserted}(t)$, the exchange kinetics would have been described by rapid (k1) and slow processes (k2). Contrarily, we considered that proton (H_3O^+) can diffuse more rapidly than Na^+ ions. Hence, the rapid insertion of protons leads to a charge accumulation at the particle level. Such a charge difference could be at the origin of the exfoliation of the layers. This result provides the first evidence of an exfoliation mechanism driven by an excess charge-based intercalation reaction. It also demonstrated that conductimetric measurements can be used to monitor kinetic parameters of reactions implying an electrolytic solution and a solid.

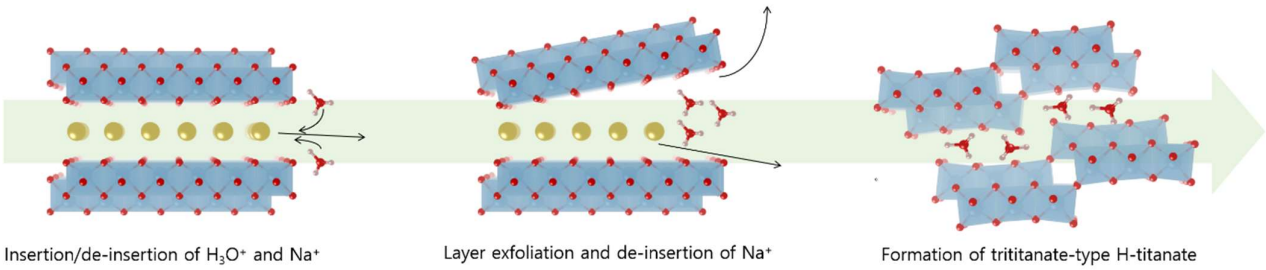

Fig. 10 Schematic representation of the intercalation-exfoliation processes from lepidocrocite-type Na-titanate to trititanate-type H-titanate.

To sum up, we provided a schematic representation of the intercalation-exfoliation processes occurring during the structural changes from lepidocrocite-type Na-titanate to trititanate-type H-titanate (**Fig. 10)**. We showed that the Na^+/H^+ ionic exchange first occurs at the surface of the particles. After the de-intercalation of surface Na^+ ions, the diffusion of Na^+ located in the inner sites is delayed compared to the fast insertion of protons. The latter induced a charge accumulation which was suggested to induce the exfoliation of the titanate layer. Concomitantly, the progressive insertion of protons induced a structural re-arrangement, which might originate from the presence of native cationic vacancies in the pristine material. As a consequence, a transition from a flat edge-sharing TiO_6 octahedra lepidocrocite toward the corrugated ribbons of edge-sharing TiO_6 octahedra was observed.

Conclusions

In this work, we investigated the reactions involved during the ionic exchange reaction between a layered Na-titanate (lepidocrocite structure) and an acidic solution (HCl). The reactions involved were investigated at the compositional/morphological and structural levels. The ionic exchange induced a structural change from the lepidocrocite to the trititanate structure as shown by real-space refinements of *ex situ* pair distribution function data. Moreover, the ionic exchange reaction induces a progressive exfoliation of the Na-titanate particles leading to 2-5 nm thin elongated crystallites. To further understand the different steps associated with the ionic exchange, we used conductimetric titration to characterize the intercalation(H^+)/de-intercalation(Na^+) reactions and assessed kinetic parameters. The latter enabled us to hypothesize the origin for the observed exfoliation of the particles, which was due to an accumulation of charges at the particle level due to the rapid intercalation of protons.

Conflicts of interest

There are no conflicts to declare.

Acknowledgements

The work done at the Advanced Photon Source, an Office of Science User Facility operated for the U.S. Department of Energy (DOE) Office of Science by Argonne National Laboratory, was supported by the U.S. DOE under contract no. DE-AC02-06CH11357. We thank IMPC FR2482 for SEM-FEG and TEM instrumentation and funded by CNRS, Sorbonne Université and C'Nano projects of Région Ile-de-France. We thank Benoît Tremblay for his help in FT-IR measurements.

Notes and references

1 M. S. Whittingham, Lithium Batteries and Cathode Materials, *Chem. Rev.*, 2004, **104**, 4271–4302.
2 J. C. Boivin and G. Mairesse, Recent Material Developments in Fast Oxide Ion Conductors, *Chem. Mater.*, 1998, **10**, 2870–2888.
3 L. Wang and T. Sasaki, Titanium Oxide Nanosheets: Graphene Analogues with Versatile Functionalities, *Chem. Rev.*, 2014, **114**, 9455–9486.
4 I. E. Grey, I. C. Madsen, J. A. Watts, L. A. Bursill and J. Kwiatkowska, New cesium titanate layer structures, *Journal of Solid State Chemistry*, 1985, **58**, 350–356.
5 T. Sasaki, M. Watanabe, Y. Michiue, Y. Komatsu, F. Izumi and S. Takenouchi, Preparation and Acid-Base Properties of a Protonated Titanate with the Lepidocrocite-like Layer Structure, *Chem. Mater.*, 1995, **7**, 1001–1007.
6 T. Sasaki, M. Watanabe, H. Hashizume, H. Yamada and H. Nakazawa, Macromolecule-like Aspects for a Colloidal Suspension of an Exfoliated Titanate. Pairwise Association of Nanosheets and Dynamic Reassembling Process Initiated from It, *J. Am. Chem. Soc.*, 1996, **118**, 8329–8335.
7 T. Gao, H. Fjellvåg and P. Norby, Protonic titanate derived from CsxTi2−x/2Mgx/2O4 (x = 0.7) with lepidocrocite-type layered structure, *J. Mater. Chem.*, 2009, **19**, 787–794.
8 R. Uppuluri, A. Sen Gupta, A. S. Rosas and T. E. Mallouk, Soft chemistry of ion-exchangeable layered metal oxides, *Chem. Soc. Rev.*, 2018, **47**, 2401–2430.
9 T. Kasuga, M. Hiramatsu, A. Hoson, T. Sekino and K. Niihara, Titania Nanotubes Prepared by Chemical Processing, *Adv. Mater.*, 1999, **11**, 1307–1311.
10 K. Nakamura, Y. Oaki and H. Imai, Monolayered Nanodots of Transition Metal Oxides, *J. Am. Chem. Soc.*, 2013, **135**, 4501–4508.
11 J. Ma, K. G. Reeves, A.-G. Porras Gutierrez, M. Body, C. Legein, K. Kakinuma, O. J. Borkiewicz, K. W. Chapman, H. Groult, M. Salanne and D. Dambournet, Layered Lepidocrocite Type Structure Isolated by Revisiting the Sol–Gel Chemistry of Anatase TiO2: A New Anode Material for Batteries, *Chem. Mater.*, 2017, **29**, 8313–8324.
12 K. Jiang, P. Xiong, J. Ji, J. Zhu, R. Ma, T. Sasaki and F. Geng, Two-Dimensional Molecular Sheets of Transition Metal Oxides toward Wearable Energy Storage, *Acc. Chem. Res.*, 2020, **53**, 2443–2455.
13 T. Sasaki, M. Watanabe, Y. Michiue, Y. Komatsu, F. Izumi and S. Takenouchi, Preparation and Acid-Base Properties of a Protonated Titanate with the Lepidocrocite-like Layer Structure, *Chem. Mater.*, 1995, **7**, 1001–1007.
14 T. Maluangnont, K. Matsuba, F. Geng, R. Ma, Y. Yamauchi and T. Sasaki, Osmotic Swelling of Layered Compounds as a Route to Producing High-Quality Two-Dimensional Materials. A Comparative Study of Tetramethylammonium versus Tetrabutylammonium Cation in a Lepidocrocite-type Titanate, *Chem. Mater.*, 2013, **25**, 3137–3146.
15 R. Ma, Y. Bando and T. Sasaki, Directly Rolling Nanosheets into Nanotubes, *J. Phys. Chem. B*, 2004, **108**, 2115–2119.
16 S. Kang, A. Singh, K. G. Reeves, J.-C. Badot, S. Durand-Vidal, C. Legein, M. Body, O. Dubrunfaut, O. J. Borkiewicz, B. Tremblay,

C. Laberty-Robert and D. Dambournet, Hydronium Ions Stabilized in a Titanate-Layered Structure with High Ionic Conductivity: Application to Aqueous Proton Batteries, *Chem. Mater.*, 2020, **32**, 9458–9469.

17 A. P. Hammersley, S. O. Svensson, M. Hanfland, A. N. Fitch and D. Hausermann, Two-dimensional detector software: From real detector to idealised image or two-theta scan, *High Pressure Research*, 1996, **14**, 235–248.

18 P. Juhás, T. Davis, C. L. Farrow and S. J. L. Billinge, PDFgetX3 : a rapid and highly automatable program for processing powder diffraction data into total scattering pair distribution functions, *J Appl Crystallogr*, 2013, **46**, 560–566.

19 C. L. Farrow, P. Juhas, J. W. Liu, D. Bryndin, E. S. Božin, J. Bloch, T. Proffen and S. J. L. Billinge, PDFfit2 and PDFgui: computer programs for studying nanostructure in crystals, *J. Phys.: Condens. Matter*, 2007, **19**, 335219.

20 J. Badot, L. Binet, N. Baffier, R. Morineau and A. Fourrier-Lamer, Electrical transport properties in vanadium bronzes obtained by the sol-gel process, *Solid State Ionics*, 1992, **53–56**, 343–350.

21 J. C. C. Chan, Spin echoes in half-integer quadrupole systems, *Concepts in Magnetic Resonance*, 1999, **11**, 363–377.

22 D. Massiot, F. Fayon, M. Capron, I. King, S. Le Calvé, B. Alonso, J.-O. Durand, B. Bujoli, Z. Gan and G. Hoatson, Modelling one- and two-dimensional solid-state NMR spectra, *Magn. Reson. Chem.*, 2002, **40**, 70–76.

23 I. Andrusenko, E. Mugnaioli, T. E. Gorelik, D. Koll, M. Panthöfer, W. Tremel and U. Kolb, Structure analysis of titanate nanorods by automated electron diffraction tomography, *Acta Cryst B*, 2011, **67**, 218–225.

24 O. V. Yakubovich and V. V. Kireev, Refinement of the crystal structure of Na2Ti3O7, *Crystallogr. Rep.*, 2003, **48**, 24–28.

25 S. J. L. Billinge and M. G. Kanatzidis, Beyond crystallography: the study of disorder, nanocrystallinity and crystallographically challenged materials with pair distribution functions, *Chem. Commun.*, 2004, 749–760.

26 K. G. Reeves, J. Ma, M. Fukunishi, M. Salanne, S. Komaba and D. Dambournet, Insights into Li^+ , Na^+ , and K^+ Intercalation in Lepidocrocite-Type Layered TiO_2 Structures, *ACS Appl. Energy Mater.*, 2018, **1**, 2078–2086.

27 A. Cadène, B. Rotenberg, S. Durand-Vidal, J.-C. Badot and P. Turq, Dielectric spectroscopy as a probe for dynamic properties of compacted smectites, *Physics and Chemistry of the Earth, Parts A/B/C*, 2006, **31**, 505–510.

28 K. S. Cole and R. H. Cole, Dispersion and Absorption in Dielectrics I. Alternating Current Characteristics, *The Journal of Chemical Physics*, 1941, **9**, 341–351.

29 J.-C. Badot and N. Baffier, Ionic Conductivity and Dielectric Properties of Vanadium Pentoxide Xerogels, *J. Mater. Chem.*, 1992, **2**, 8.

30 R. Buchner, J. Barthel and J. Stauber, The dielectric relaxation of water between 0°C and 35°C, *Chemical Physics Letters*, 1999, **306**, 57–63.

31 S. Mukherjee, The effect of chemically preintercalated alkali ions on the structure of layered titanates and their electrochemistry in aqueous energy storage systems, *Journal of Materials Chemistry A*, 2020, **8**, 18220–18231.

32 S. Fleischmann, Y. Sun, N. C. Osti, R. Wang, E. Mamontov, D. Jiang and V. Augustyn, Interlayer separation in hydrogen titanates enables electrochemical proton intercalation, *J. Mater. Chem. A*, 2020, **8**, 412–421.

33 M. A. Tsiamtsouri, P. K. Allan, A. J. Pell, J. M. Stratford, G. Kim, R. N. Kerber, P. C. M. M. Magusin, D. A. Jefferson and C. P. Grey, Exfoliation of Layered Na-Ion Anode Material $Na_2Ti_3O_7$ for Enhanced Capacity and Cyclability, *Chem. Mater.*, 2018, **30**, 1505–1516.

34 M. Gateshki, Q. Chen, L.-M. Peng, P. Chupas and V. Petkov, Structure of nanosized materials by high-energy X-ray diffraction: study of titanate nanotubes, *Zeitschrift für Kristallographie - Crystalline Materials*, , DOI:10.1524/zkri.2007.222.11.612.

35 M. A. Tsiamtsouri, P. K. Allan, A. J. Pell, J. M. Stratford, G. Kim, R. N. Kerber, P. C. M. M. Magusin, D. A. Jefferson and C. P. Grey, Exfoliation of Layered Na-Ion Anode Material Na2Ti3O7 for Enhanced Capacity and Cyclability, *Chem. Mater.*, 2018, **30**, 1505–1516.

36 J. C. Pérez-Flores, F. García-Alvarado, M. Hoelzel, I. Sobrados, J. Sanz and A. Kuhn, Insight into the channel ion distribution and influence on the lithium insertion properties of hexatitanates A2Ti6O13 (A = Na, Li, H) as candidates for anode materials in lithium-ion batteries, *Dalton Trans.*, 2012, **41**, 14633–14642.

37 F. Angeli, O. Villain, S. Schuller, S. Ispas and T. Charpentier, Insight into sodium silicate glass structural organization by multinuclear NMR combined with first-principles calculations, *Geochimica et Cosmochimica Acta*, 2011, **75**, 2453–2469.

38 V. Laperche, J. F. Lambert, R. Prost and J. J. Fripiat, High-resolution solid-state NMR of exchangeable cations in the interlayer surface of a swelling mica, https://pubs.acs.org/doi/pdf/10.1021/j100388a015, (accessed January 23, 2021).

39 R. Nanda, G. M. Bowers, N. Loganathan, S. D. Burton and R. J. Kirkpatrick, Temperature dependent structure and dynamics in smectite interlayers: 23Na MAS NMR spectroscopy of Na-hectorite, *RSC Adv.*, 2019, **9**, 12755–12765.

40 M. D. Alba, A. Cota, F. J. Osuna, E. Pavón, A. C. Perdigón and F. Raffin, Bionanocomposites based on chitosan intercalation in designed swelling high-charged micas, *Scientific Reports*, 2019, **9**, 10265.

41 Y. Liu, J. Tossell and H. Nekvasil, A theoretical study of structural factors correlated with 23Na NMR parameters, *American Mineralogist*, 2004, **89**, 1314–1322.

42 M. Crocker, R. H. M. Herold, A. E. Wilson, M. Mackay, C. A. Emeis and A. M. Hoogendoorn, 1 H NMR spectroscopy of titania. Chemical shift assignments for hydroxy groups in crystalline and amorphous forms of TiO2, *J. Chem. Soc., Faraday Trans.*, 1996, **92**, 2791–2798.

43 M. Wang, N. R. Jaegers, M.-S. Lee, C. Wan, J. Z. Hu, H. Shi, D. Mei, S. D. Burton, D. M. Camaioni, O. Y. Gutiérrez, V.-A. Glezakou, R. Rousseau, Y. Wang and J. A. Lercher, Genesis and Stability of Hydronium Ions in Zeolite Channels, *J. Am. Chem. Soc.*, 2019, **141**, 3444–3455.

44 M. M. Mortland and J. L. Mellor, Conductometric Titration of Soils for Cation-Exchange Capacity1, *Soil Science Society of America Journal*, 1954, **18**, 363.

45 M. Ranđelović, M. Purenović, J. Purenović and M. Momčilović, Removal of Mn^{2+} from water by bentonite coated with immobilized thin layers of natural organic matter, *Journal of Water Supply: Research and Technology-Aqua*, 2011, **60**, 486–493.

46 J.-F. Dufrêche, O. Bernard, S. Durand-Vidal and P. Turq, Analytical Theories of Transport in Concentrated Electrolyte Solutions from the MSA, *J. Phys. Chem. B*, 2005, **109**, 9873–9884.

47 G. M. Roger, S. Durand-Vidal, O. Bernard and P. Turq, Electrical Conductivity of Mixed Electrolytes: Modeling within the Mean Spherical Approximation, *J. Phys. Chem. B*, 2009, **113**, 8670–8674.

48 D. V. Bavykin and F. C. Walsh, Kinetics of Alkali Metal Ion Exchange into Nanotubular and Nanofibrous Titanates, *J. Phys. Chem. C*, 2007, **111**, 14644–14651.

49 T. Dickenson and A. Fiennes, *Chemical Kinetics*, Pergamon, 1966.